

X-Fi: A MODALITY-INVARIANT FOUNDATION MODEL FOR MULTIMODAL HUMAN SENSING

Xinyan Chen, Jianfei Yang*

MARS Lab, Nanyang Technological University

ABSTRACT

Human sensing, which employs various sensors and advanced deep learning technologies to accurately capture and interpret human body information, has significantly impacted fields like public security and robotics. However, current human sensing primarily depends on modalities such as cameras and LiDAR, each of which has its own strengths and limitations. Furthermore, existing multi-modal fusion solutions are typically designed for fixed modality combinations, requiring extensive retraining when modalities are added or removed for diverse scenarios. In this paper, we propose a modality-invariant foundation model for all modalities, X-Fi, to address this issue. X-Fi enables the independent or combinatory use of sensor modalities without additional training by utilizing a transformer structure to accommodate variable input sizes and incorporating a novel “X-fusion” mechanism to preserve modality-specific features during multimodal integration. This approach not only enhances adaptability but also facilitates the learning of complementary features across modalities. Extensive experiments conducted on the MM-Fi and XRF55 datasets, employing six distinct modalities, demonstrate that X-Fi achieves state-of-the-art performance in human pose estimation (HPE) and human activity recognition (HAR) tasks. The findings indicate that our proposed model can efficiently support a wide range of human sensing applications, ultimately contributing to the evolution of scalable, multimodal sensing technologies.

1 INTRODUCTION

Human sensing refers to using various sensors to capture human body information in a specific space, such as presence (Nguyen et al., 2016; Nanzer, 2017), activity (Vrigkas et al., 2015; Yang et al., 2023)), and pose (Toshev & Szegedy, 2014; Cai et al., 2022). Benefiting from advanced deep learning technology, human sensing has made significant progress in both accuracy and granularity, expanding applications in many domains. For instance, video surveillance (Elharrouss et al., 2021) is empowered by human sensing algorithms to analyze dangerous behaviors. In the field of robotics, human pose helps robots comprehend human actions and then realize human-robot collaboration (Gao et al., 2019).

Currently, human sensing tasks mainly rely on vision-based modalities like cameras (Ionescu et al., 2013), which face inherent limitations such as reliance on illumination, privacy concerns, and insufficient 3D information (Cai et al., 2022). Alternative modalities like LiDAR, mmWave radar, and WiFi have been introduced to overcome these challenges (Nirmal et al., 2021). Each modality has distinctive advantages but also has limitations, e.g., LiDAR offers high-resolution data but is expensive (Li et al., 2022), mmWave radar is cost-effective and informative but lacks sensitivity to static objects (An & Ogras, 2021), and WiFi is ubiquitous and privacy-preserving but has low resolution (Yang et al., 2023; Zhou et al., 2023). Therefore, single-modal sensing solutions cannot fit all scenarios, and a multi-modal approach that leverages the strengths of each modality is essential for future advancements in human sensing.

Numerous methods have been proposed for multi-modal perception based on sensor fusion. They usually predefine a fixed set of modalities for a specific scenario, e.g., combining RGB and LiDAR

* Jianfei Yang is the corresponding author (jianfei.yang@ntu.edu.sg).

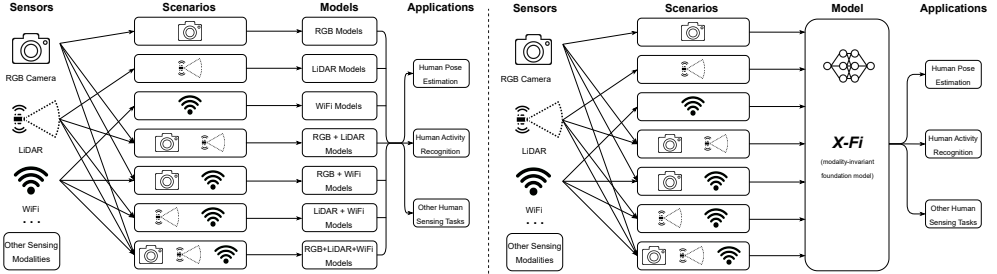


Figure 1: The left image shows existing modality-corresponding human sensing solutions, while the right image illustrates our proposed modality-invariant foundation model, X-Fi, which enables modality-invariant human sensing.

for pose estimation in autonomous driving to enhance long-range all-day sensing. Nevertheless, in any given scenario, once the model is trained, adding or removing even one modality requires a huge effort: adjusting the network and retraining it from scratch. In the real world, we may require versatile combinations of sensor modalities according to different scenarios (Yang et al., 2024). Hence, we contemplate whether it is possible to design a **one-for-all solution for modality-invariant human sensing**. Such a model would require training only once, allowing all sensor modalities that participated in the training process to be utilized independently or in any combination for a wide range of potential applications.

To achieve modality-invariant human sensing, we aim to design a foundation model that can dynamically handle varying numbers of modalities. First, considering the arbitrary number of input modalities, we naturally resorted to a transformer structure due to its adaptability to variable input sizes. Second, recognizing that each modality has unique characteristics, we adopt modality-specific feature extractors to capture distinctive information. Finally, to retain each modality’s distinct features during multimodal fusion, we introduced a cross-attention fusion mechanism that reduces the information loss caused by multi-modal feature compression and fusion process. Surprisingly, this design not only supports dynamic inputs from various modalities but by training with diverse modality combinations to perform sensing tasks, it learns complementary features among modalities as well. As a result, it even achieves superior performance against conventional modality fusion methods such as feature-level and decision-level fusion.

To this end, we propose a novel modality-invariant foundation model, X-Fi, for versatile human sensing. X-Fi can take in any combinations of modalities and activate corresponding parts to extract modality-specific features. A cross-modal transformer is designed to learn a cross-modal feature and each modality information is then preserved in the representation by executing cross-attention multi-modal fusion processes to preserve distinctive modal features. As shown in Figure.2, we have a set of modality-corresponded feature encoders and key-value generators to extract, fine-tune and preserve modality-specific features. For versatile combinations of sensor modalities, corresponding feature encoders are activated to obtain modality-specific features of each modality. Subsequently, the attention-based key-value generators are trained to produce key-value pairs, which contain more task-related information derived from modality-specific features (Vaswani et al., 2017). For the modality-invariant multi-modal fusion process, we introduce “X-fusion” block. It consists of a cross-modal transformer and a set of modality-correlated cross-attention transformers. The cross-modal transformer is designed to adaptively learn a unified embedding across variable-sized multi-modal embedding, which comprises the features of each modality. The generated cross-modal embedding serves as the query, along with key-value pairs of each modality, are sent to the corresponding cross-attention transformer to perform attention-based feature injection. We evaluated X-Fi on human pose estimation (HPE) and human activity recognition (HAR) tasks in MM-Fi (Yang et al., 2024) and XRF55 (Wang et al., 2024), demonstrated that X-Fi surpasses previous methods by MPJPE 24.8% and PA-MPJPE 21.4% on HPE task, 2.8% on HAR task.

The main contributions are summarized as follows. First, we proposed X-Fi, a foundation model for modality invariant human sensing, which has strong scalability that only needs to be trained once and could support dynamic inputs from various modalities for a wide range of sensing scenarios. Second, we further developed X-Fusion block to empower efficient multi-modal fusion under modality invariant training strategy by preserving modality-specific information and applying token fusion technique to inject back into the cross-modal embedding. Third, we conducted extensive experi-

ments on the MM-Fi and XRF55 datasets, utilizing a total of six distinct modalities, and observed that our proposed X-Fi achieved state-of-the-art performance on both the HPE and HAR tasks.

2 RELATED WORK

2.1 HUMAN SENSING

Human sensing has been extensively explored for applications such as autonomous driving and robotics in recent years, aiming to capture, analyze, and interpret human body information through various sensors and novel deep learning frameworks (Cai et al., 2022). Most human sensing approaches could generally be split into three categories: i) Vision-based approaches, where human body information is extracted from visual data captured by cameras (Shahroury et al., 2016) and leveraged by deep learning architectures like convolutional structures (Chun et al., 2018; Pavlakos et al., 2018; Sun et al., 2019; Li et al., 2020) and transformer (Goel et al., 2023; Cai et al., 2024; Qiu et al., 2022). ii) Sensor-based approaches, using alternative modalities such as LiDAR (Ren et al., 2024), mmWave radar (Wang et al., 2021; An & Ogras, 2022), and WiFi CSI (Yang et al., 2023; Zhou et al., 2023) to overcome limitations of vision-based methods and expand applicability. iii) Multimodal fusion approaches, including decision-level fusion (An et al., 2022; Yang et al., 2024) and feature-level fusion (Zheng et al., 2022; Chen et al., 2023), which combine each modality’s strengths to improve sensing performance.

2.2 MODALITY-INVARIANT METHODS

Current human sensing methods lack broad applicability. Both decision-level fusion approaches (Yang et al., 2024) and feature-level fusion approaches (Zheng et al., 2022; Chen et al., 2023) are typically tailored to fixed modality combinations for specific applications. For example, (Zheng et al., 2022) developed a specific heatmap sampling structure to fuse 2D heatmaps from RGB images with projected 2D point clouds from LiDAR. Similarly, (Chen et al., 2023) employed modality-specific backbones to extract grid features from images and cluster features from mmWave point clouds, combining them via a global integration module to produce fused features.

In fields beyond human sensing, several studies on multimodal fusion seek to accommodate diverse sensor inputs to a unified model for various applications. Some methods align all input modalities with a primary modality (Man et al., 2023; Han et al., 2024), like OneLLM, which employs a universal encoder and projection module to tokenize eight modalities and align the resulting multimodal tokens with language using large language models (Han et al., 2024), but these approaches heavily rely on the presence of the primary modality. Some other methods, such as (Xue & Marculescu, 2023), design a gating network to identify the active input modalities and subsequently activate the modality-combination-specific expert networks for multimodal fusion. Yet, this approach is struggled by the necessity of creating numerous expert networks to accommodate a wide range of potential modal combinations in the presence of an extensive sensor options. Other methods like (Memmel et al., 2023) utilize a transformer-based structure to process tokenized input and also introduce a modality-invariant training strategy by dropping modalities during training. However, this approach is only applicable when the input modalities are limited to vision-based modalities.

3 MODALITY-INVARIANT FOUNDATION MODEL FOR HUMAN SENSING

Assume that input X comprises a random combination of modalities within a specific range, including any number and type of modalities. Our objective is to learn a unified representation Emb_{cm} that integrates modality-specific features from X by using a modality-invariant foundation model \mathcal{F} . This representation can be mapped to various down-stream human sensing task spaces by using corresponding task-specific functions g_{t_i} , such that the task-specified loss function $\mathcal{L}_{t_i}(g_{t_i}(\mathcal{F}(X)); y_{t_i})$ is minimized. Thus we propose X-Fi, a modality-invariant human sensing framework designed to map the arbitrary multimodal input X to any task-specific target domain t_i , such as HPE and HAR.

As illustrated in Fig 2, given N modalities in the dataset, we first prepare a set of modality-specified feature encoders $\{Enc_i(\cdot; \theta_{Enc,i})\}_{i=1}^N$ to extract features $\{F_i \in \mathbb{R}^{n_f \times d_f}\}_{i=1}^N$ from corresponding modality inputs $\{x_i\}_{i=1}^N$. Then we introduce cross-attention-based multi-modal fusion design that

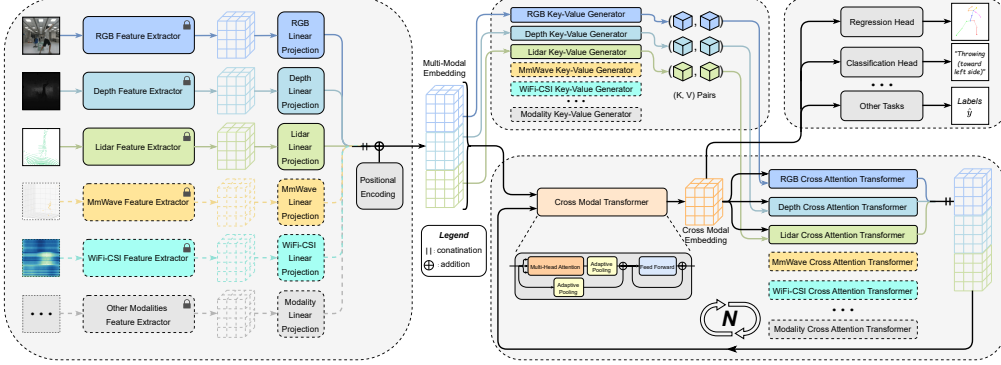


Figure 2: The architecture of the proposed modality-invariant foundation model, X-Fi. The X-Fi consists of a modality feature encoding module that extracts modality-specific features, and a X-Fusion modules that learns an unified cross-modal feature through modality-fusion in the Cross Modal Transformer and preserves distinctive modal features through feature injection in modality-specified Cross Attention Transformers.

could efficiently preserve modality-specific features in the learned unified cross-model embedding. The modality-specified key-value generators $\{G_{kv,i}(\cdot; \theta_{G,i}^{kv})\}_{i=1}^N$ are applied to encode the modality information from $\{F_i\}_{i=1}^N$ into key-value pairs $\{(K_i, V_i)\}_{i=1}^N$. To obtain an unified cross modal embedding $Emb_{cm} \in \mathbb{R}^{n_f \times d_f}$, we use a cross modal transformer $G_{cm}(\cdot; \theta_G^{cm})$ to learn from the $Emb_{mm} \in \mathbb{R}^{(n_f * N) \times d_f}$. The generated cross modal embedding Emb_{cm} serves as the query Q , together with each key-value pair, to send into the modality-corresponded cross attention transformer $\{G_{ca,i}(\cdot; \theta_{G,i}^{ca})\}_{i=1}^N$ in order to inject modality-specific information. Through iterative learning of the Emb_{cm} and performing modality-specific information injection, the final produced Emb_{cm} could be used for various downstream tasks via task-correlated Multi-layer Perceptron (MLP) head.

In the following subsections, we will decompose X-Fi by describing the modality feature encoding (sec. 3.1), the attention-based X-Fusion (sec. 3.2), and the modality-invariant training (sec. 3.3).

3.1 MODALITY FEATURE ENCODING

In human sensing, different modalities exhibit distinctive characteristics, requiring unique feature encoder structures to extract robust modality-specific features. For instance, images are represented as a 2D matrix and have rich spatial feature, requiring models like CNN (LeCun et al., 1998) and ViT (Dosovitskiy et al., 2021) to extract vision features. While point clouds from LiDAR consist of a set of unordered points in Euclidean space, necessitating point cloud-specific frameworks like Point Net (Qi et al., 2017) and Point Transformer (Zhao et al., 2021) to process them. Thus, we introduce modality-specific feature encoders in X-Fi to extract features from various modalities.

In X-Fi, the modality-specified feature encoder $Enc_i(\cdot; \theta_{Enc,i})$ for each modality consists of a pre-trained feature extractor $E_i(\cdot; \theta_{E,i})$ and a linear projection head. The feature extractors are responsible for extracting informative high-dimensional representations from modal data. To accommodate diverse combinations of sensor modalities across different application scenarios, we can select any model structures as backbones for these feature extractors. Each feature extractor is modality specified, which allows us to choose a model structure that best aligns with the unique characteristics of the modality’s data, thereby ensuring the efficiency of feature extraction. For example: for point clouds from mmWave radar and LiDAR, we adopt the Point Transformer backbone (Zhao et al., 2021). The self-attention mechanism in Point Transformers is particularly suitable for point cloud data due to its permutation invariance and ability to dynamically focus on relevant points.

Since the data structures of the features extracted by different modality-specific feature extractors are still different across modalities, we use a set of linear projection structures to unify these features into the same dimensional space, allowing them to be used together in subsequent stages of the model. Finally, the positional encoding is added to obtain the final features.

$$\{Enc_i(\cdot; \theta_{Enc,i})\}_{i=1}^N = \{\text{LinearProjection}_i(E_i(\cdot; \theta_{E,i}); \theta_{LP,i})\}_{i=1}^N \quad (1)$$

3.2 ATTENTION-BASED X-FUSION

After obtaining the modality-specific features, a natural question is posed: How can the modality-invariant foundation model effectively combine these features to obtain a unified cross-modal representation that is applicable for downstream human sensing tasks? Thus, in this section, we will interpret the proposed X-Fusion structure which consists of a cross-modal transformer to learn an unified cross-modal feature and cross-attention multi-modal fusion modules to preserve distinctive modality features.

3.2.1 CROSS-MODAL TRANSFORMER

In this subsection, we aim to learn a unified cross-modal feature. The proposed structure should be capable of dynamically handling varying numbers of modality features and effectively achieving information interaction among diverse modal features. Thus, we adopt a Transformer-based structure (Vaswani et al., 2017) that can accept variable sizes of input. Also, the self-attention mechanism can equally learn the long-distance dependencies between any two modal features in the input, thereby effectively modeling global information for all modal features.

First, we concatenate all obtained modality-specific features to initialize a multi-modal embedding $Emb_{mm} \in \mathbb{R}^{(n_f * N) \times d_f}$. As illustrated in the Figure. 2, we then linearly map the multi-modal embedding into three vectors, named Q_{mm}, K_{mm}, V_{mm} . Next, we perform dot-product-based multi-head attention to calculate the attention value which models the dependencies among modality features.

Notably, The multi-head attention and feed-forward blocks output embedding of the same size as the input, resulting in variable-sized cross-modal embedding based on the number of modality inputs. This variability complicates the design of subsequent fusion blocks and task-specific projection heads which have fixed-size parameters. To address this issue, we apply adaptive pooling both after the multi-head attention block and within the residual connection to perform down sampling and obtain unified-sized outputs $Z_{mm} \in \mathbb{R}^{n_f \times d_f}$. Finally, we feed Z_{mm} into a feed-forward structure with a residual connection to obtain the unified cross-modal embedding $Emb_{cm} \in \mathbb{R}^{n_f \times d_f}$.

$$Z_{mm} = \text{AvgPool}(\text{MultiHead}(Q_{mm}, K_{mm}, V_{mm})) + \text{AvgPool}(Emb_{mm}) \quad (2)$$

$$Emb_{cm} = \text{FFN}(Z_{mm}) + Z_{mm} \quad (3)$$

3.2.2 CROSS-ATTENTION MULTI-MODAL FUSION

However, the basic transformer design, which has a layered architecture with sequentially stacked transformer blocks, often leads to a prioritization of dominant modalities. First reason is that the self-attention mechanism in the cross-modal transformer tends to assign higher attention weights to the more informative modality-specific features (Lu et al., 2019), causing significant information loss from less dominant modalities. Secondly, in layered structures, different layers focus on distinct aspects of the input data, and later layers naturally exerting a greater influence on the overall output. As a result, the modalities emphasized by the later layers tend to be disproportionately prioritized. To efficiently and equally fuse features from any combination of modalities, we develop a cross-attention multi-modal fusion architecture that ensures the model pays equal attention to every input modality by incorporating modality-specific information into the cross-modal embedding. We also design an X-Fusion process that iterates on the same block, compelling the X-Fusion block to identify a unified dynamic attention allocation method that effectively preserves the features of each modality and optimally integrates them to achieve the most optimal solution.

Key-Value Generators. To prepare key-value pairs that preserve modality-specific information, we design key-value generators for each modality. take the i -th modality for illustration, key-value generator $G_{kv,i}$ receives modality specific feature $F_i \in \mathbb{R}^{n_f \times d_f}$ extracted from feature extractor E_i as the input. F_i is first passed through a two-layer MLP with a hidden dimension of $d_f * 2$ incorporating a Rectified Linear Unit (ReLU) activation (Nair & Hinton, 2010) and layer normalization in between. The MLP output is then projected to key K_i and value V_i using separate linear mapping layers. Once the key-value pair (K_i, V_i) is generated from F_i , it remains unchanged during iterations in the X-fusion block to prevent information leakage between modalities.

Cross-Attention Transformers. We employ a series of cross-attention transformers to integrate modality-specific information into the cross-modal embedding Emb_{cm} . Each transformer is associated with a specific modality and receives three inputs: the unified cross-modal embedding Emb_{cm} that is shared across all cross-attention transformers, the key (K) and value (V) pairs obtained from modality-specific key-value generators. Take the i -th modality as an example, Emb_{cm} serves as the query (Q) in the multi-head attention mechanism. Attention weights are computed based on Q and K_i to scale the modality-specific value V_i , yielding an intermediate result denoted as O_i . Subsequently, Emb_{cm} is residual added to O_i to retain cross-modal features, resulting in O'_i . The final output F'_i of each modality-specific cross-attention transformer is produced by passing O'_i through a feed-forward structure with a residual connection. Each F'_i generated from modality-specific cross-attention transformer encapsulates fused information focusing on a single modality. To integrate information from all modalities, we concatenate all $\{F'_i\}_{i=1}^N$ to get the updated multi-modal embedding Emb'_{mm} , which is used in the subsequent X-fusion block iteration.

$$Emb'_{mm} = \text{Concat}\{G_{ca,i}(Emb_{cm}, K_i, V_i; \theta_{G,i}^{ca})\}_{i=1}^N \quad (4)$$

3.3 MODALITY-INVARIANT TRAINING

To train our modality invariant foundation model, we design an explicit training strategy with reference to (Memmel et al., 2023). First, to ensure that the feature extractors retain their ability to capture modality-specific features without being biased, we pre-train the parameters on the respective datasets and freeze these parameters during subsequent training. Next, to simulate versatile combinations of sensor modalities in different scenarios, we use a modality existence list containing n elements to indicate whether each modality is present in the input modal combination. This modality existence list is utilized to control the presence of input modalities during each training iteration and activate the corresponding modality-specific structures in the X-Fi. In addition, each modality is assigned an independent occurrence probability p_i . By adjusting the modality-corresponded p_i , we can refine the model’s training strategy by prioritizing certain modalities. For example, because LiDAR point cloud data is inherently sparser than image data and exhibits complex features such as permutation invariance, it is necessary to include more LiDAR samples in the training process to ensure accurate model fitting. Since the training sample is controlled by the modality existence list, we can model the training samples by the distribution of the modality existence list. We denote the count of occurrences of i -th modality in m training iterations by a variable K_i , and $K_i \sim \text{Binomial}(m, p_i)$. Since K_i for each modality is independent, we can describe the distribution using a joint probability mass function $P(K_1 = k_1, \dots, K_n = k_n) = \prod_{i=1}^n \binom{m}{k_i} p_i^{k_i} (1 - p_i)^{m - k_i}$. For each training batch, the modality existence list is sampled from a distribution to regulate the input modalities, thereby influencing the activation of modality-specific model structures.

4 EXPERIMENTS

4.1 EXPERIMENTAL SETUP

Datasets. We train and evaluate our proposed X-Fi on two largest human sensing multimodal public datasets MM-Fi (Yang et al., 2024) and XRF55 (Wang et al., 2024), to assess its efficiency as a unified modality-invariant foundation model across diverse human sensing tasks, including Human Pose Estimation (HPE) and Human Activity Recognition (HAR). The details of the specific datasets utilized for each task are provided as follows. (i) HPE: MM-Fi consists of over 320k synchronized frames from 40 human subjects. Each synchronized frame consists of samples collected from 5 sensing modalities, including RGB images (I), Depth images (D), LiDAR point clouds (L), mmWave point clouds (R), and WiFi-CSI (W). The chosen annotation type is 3D whole-body keypoints, representing the positions of 17 human joints. (ii) HAR: MM-Fi and XRF55 are utilized for HAR task evaluation. MM-Fi consists of 27 action categories, including 14 daily activities and 13 rehabilitation exercises. We exclude WiFi-CSI modality from MM-Fi when addressing the HAR task, as each WiFi data sample spans only 100ms, which is insufficient to effectively capture the distinct data patterns associated with different actions. XRF55 includes 42.9K radio frequency samples collected by 3 sensing modalities, including mmWave Range-Doppler & Range-Angle Heatmaps (R), WiFi-CSI (W), and RFID phase series data (RF). XRF55 comprises 55 action classes collected from 39 human subjects, covering categories such as fitness activities and human-computer interactions.

MM-Fi		MPJPE				PA-MPJPE				
modality	X-Fi	Baseline1	Imp↓	Baseline2	Imp↓	X-Fi	Baseline1	Imp↓	Baseline2	Imp↓
I	93.9	121.0	22.4%	121.0	22.4%	60.3	68.0	11.4%	68.0	11.4%
D	101.8	102.4	0.6%	102.4	0.6%	48.4	52.7	8.2%	52.7	8.2%
L	167.1	161.5	-3.5%	161.5	-3.5%	103.2	103.5	0.3%	103.5	0.3%
R	127.4	141.3	9.8%	141.3	9.8%	69.8	72.4	3.7%	72.4	3.7%
W	225.6	227.1	0.7%	227.1	0.7%	105.3	108.0	2.5%	108.0	2.5%
I+D	86.1	96.7	11.0%	109.2	21.2%	48.1	53.9	10.7%	57.1	15.6%
I+L	93.0	122.1	23.8%	121.2	23.3%	59.7	75.6	21.1%	73.0	18.2%
I+R	88.8	101.0	12.1%	140.6	36.8%	57.3	57.3	0.0%	68.2	16.0%
I+W	93.0	146.4	36.5%	156.7	40.7%	59.5	77.3	23.1%	86.3	31.1%
D+L	102.5	111.7	8.2%	108.0	5.1%	48.4	68.8	29.7%	55.8	13.3%
D+R	98.0	94.1	-4.1%	116.4	15.8%	47.3	51.8	8.6%	57.0	17.0%
D+W	101.8	141.7	28.1%	155.5	34.5%	48.1	71.4	32.6%	81.5	41.0%
L+R	109.8	116.4	5.7%	137.0	19.9%	63.4	71.5	11.3%	71.9	11.8%
L+W	159.5	167.1	4.5%	206.2	22.6%	102.7	100.7	-2.0%	109.3	6.0%
R+W	117.2	144.2	18.7%	141.3	17.0%	62.7	72.2	13.0%	77.6	19.1%
I+D+L	84.8	102.9	17.5%	104.5	18.8%	48.2	62.3	22.7%	61.2	21.4%
I+D+R	83.4	86.7	3.8%	113.4	26.5%	47.3	50.1	5.4%	58.0	18.4%
I+D+W	85.3	118.6	28.0%	137.8	38.1%	48.1	63.7	24.4%	75.3	36.1%
I+L+R	88.4	101.4	12.8%	135.0	34.5%	57.2	62.7	8.8%	67.7	15.6%
I+L+W	93.0	134.9	31.1%	156.2	40.5%	59.7	82.0	27.2%	84.8	29.6%
I+R+W	88.5	116.5	24.1%	128.9	31.3%	57.1	63.1	9.5%	75.0	23.9%
D+L+R	96.0	95.3	-0.8%	111.3	13.7%	47.3	58.6	19.2%	58.4	19.0%
D+L+W	102.0	130.7	22.0%	154.6	34.0%	48.1	78.1	38.4%	84.1	42.8%
D+R+W	97.0	113.2	14.3%	132.0	26.5%	47.1	59.4	20.7%	71.8	34.3%
L+R+W	107.4	129.6	17.2%	141.6	24.1%	63.1	78.1	19.2%	77.0	18.1%
I+D+L+R+W	83.7	103.0	18.8%	128.9	35.1%	47.6	62.4	23.8%	72.5	34.3%

Table 1: Performance comparisons of X-Fi with baseline methods on the MM-Fi dataset for HPE task. ‘‘Baseline1’’ denotes the decision-level fusion results and ‘‘Baseline2’’ denotes the feature-level fusion results. Imp denotes the improvement achieved over baseline in percentage level.

Training Objective. Different loss functions are applied as the training objectives for different human sensing tasks. For HPE, Mean-Squared-Error is chosen as the loss function, which measures the average squared euclidean distance between each of the 17 predicted whole-body key-points and their corresponding ground truth points in 3D space. For HAR, Cross-Entropy loss is applied between the predicted probability distribution and the ground truth distribution.

Baseline Formulation. To evaluate the performance of our proposed unified modality-invariant foundation model across various human sensing tasks and modality combinations, we formulate baseline models by adopting a feature fusion approach (Das et al., 2021; Marcard et al., 2016) and a decision-level fusion approach (Yang et al., 2024). For the feature fusion approach, first, we leverage the pre-trained modality-specific feature extractors in X-Fi to obtain features from each modality. Subsequently, for single-modal inputs, a MLP structure is applied to project the single-modal features into the task representation space. For multi-modal inputs, we concatenate the features from each modality to create a multi-modal feature, which is then processed by a MLP head with an average pooling layer to fuse and map the multi-modal features into the unified task representation space. We train a baseline model for each modality combination. And for different tasks, we optimize the parameters of each baseline model (including the pre-trained feature extractor) using different learning objectives. For the decision-level fusion approach, we first obtain the final-layer output of each individual modality. Then, we calculate the average of the outputs from all modalities in the combination to generate the fused output. The baseline results are presented in the Table 1& 2.

Implementation Details. We conduct experiments on all humans sensing tasks and datasets with the following model settings. To standardize feature representations obtained by various modality-specific feature extractors, we apply linear projection units to map each modality feature representation to 32 features, each with feature dimension of 512. The positional embedding, derived from LiDAR 3D point cloud raw data due to its inherent capture of human body spatial information, is only provided in the multi-modal embedding if the LiDAR modality is present in the input. The

backbone for both the cross-modal transformer and each modality-specific cross-attention transformer consists of a 1-layer decoder-only transformer structure with 8 multi-head attention heads and a scaling factor of 0.125. Each modality-specific key-value pair and the cross-modal embedding in X-Fusion block comprise 32 features with feature dimension of 512. The AdamW optimizer, with an initial learning rate of $1 \times e^{-3}$ for HPE and $1 \times e^{-4}$ for HAR, is chosen for model optimization. The training process is performed with a batch size of 16 on an NVIDIA GeForce RTX 4090 GPU.

4.2 QUANTITATIVE RESULTS

We compare our approach with the baseline methods regarding the performance on downstream human sensing tasks, including HPE and HAR. For convenience, we refer to the decision-level fusion baseline as “baseline1”, and the feature-level fusion baseline as “baseline2”. The results for X-Fi, as shown in Tables 1 & 2, represent average values obtained from multiple experiments. These values are derived by validating the performance of a single X-Fi model across different modality combinations that is trained using the proposed modality-invariant training strategy.

Human Pose Estimation. We assess the performance of X-Fi on the MM-Fi dataset (Yang et al., 2024) by adopting two commonly-used metrics in HPE: Mean Per Joint Position Error (MPJPE) and Procrustes Analysis MPJPE (PA-MPJPE). For single-modal inputs, X-Fi improves the averaged MPJPE and PA-MPJPE by 6.0% and 5.2%, respectively. For the dual-modality inputs, the averaged MPJPE and PA-MPJPE are improved respectively by 14.5% and 14.8% on baseline1, 23.7% and 18.9% on baseline2. Notably, for LiDAR and WiFi modalities, when used as individual inputs, X-Fi does not achieve good performance, with MPJPE difference of -3.5% and $+0.7\%$, respectively. However, when the two modalities are combined as inputs, the performance improves significantly, surpassing the baseline1 by 4.5% and the baseline2 by 22.6%. For the combined input of three modalities, X-Fi demonstrates an average improvement of 17.0% and 28.8% in MPJPE, 19.5% and 25.9% in PA-MPJPE. For the combined input of four modalities, the results indicate an average enhancement of 17.0% and 35.5% in MPJPE, 21.6% and 30.8% in PA-MPJPE. For all five modalities combined input, MPJPE increases by 18.8% and 35.1%, PA-MPJPE increases by 23.8% and 34.3%.

Human Activity Recognition. The performance of X-Fi on the HAR task is evaluated by classification accuracy on both the MM-Fi (Yang et al., 2024) and XRF55 (Wang et al., 2024) datasets. On the MM-Fi dataset, X-Fi performs better than the baseline when handling multi-modal inputs, yielding an average improvement of 2.8%. But when dealing with single-modality inputs, its performance declines, dropping by 2.8%. On the XRF55 dataset, X-Fi only encounters challenges with WiFi-CSI single-modality input. It outperforms the baseline on all other modality combinations, achieving an average improvement of 6.7%. Notably, while X-Fi’s performance is suboptimal when using WiFi as a single input, when combined with other modalities, WiFi not only avoids hindering performance but also introduces unique information that enhances classification accuracy. For example, when X-Fi processes mmWave radar and RFID multimodal input, it outperforms the baseline by 15.1%. With the inclusion of WiFi, this improvement increases to 19.2%.

4.3 ANALYTICS

Impact of modality existence list. To assess the impact of adjusting the independent existing probability of each modality in the modality existence list, we conduct experiments with different probability combinations on the XRF55 dataset for the HAR task. The XRF55 modality existence list contains the independent existence probabilities of mmWave Radar, WiFi-CSI, and RFID modalities in sequential order. As shown in Table 3, X-Fi encounters difficulties in dealing with WiFi-CSI. However, through gradually increase the exist probability of WiFi-CSI, the model is prioritised to fit WiFi-CSI modality during training, which yields significant improvement from 29.1% to 55.7%

Table 2: HAR performance on the MM-Fi and XRF55 datasets.

Modality	Baseline	X-Fi	Imp \uparrow
MM-Fi			
I	25.3%	26.5%	1.2%
D	49.9%	48.1%	-1.8%
L	63.9%	52.7%	-11.2%
R	85.0%	85.7%	0.7%
I + D	45.2%	45.3%	0.1%
I + L	23.8%	35.2%	11.4%
I + R	66.9%	73.4%	6.6%
D + L	49.7%	51.6%	1.9%
D + R	74.1%	79.8%	5.7%
L + R	85.6%	88.7%	3.2%
I + D + L	43.0%	48.7%	5.7%
I + D + R	69.1%	70.7%	1.6%
I + L + R	68.2%	77.8%	9.6%
D + L + R	72.9%	80.5%	7.6%
I+D+L+R	72.6%	72.2%	-0.4%
XRF55			
R	82.1%	83.9%	1.9%
W	77.8%	55.7%	-22.1%
RF	42.2%	42.5%	0.3%
R+W	86.8%	88.2%	1.4%
R+RF	71.4%	86.5%	15.1%
W+RF	55.6%	58.1%	2.6%
R+W+RF	70.6%	89.8%	19.2%

in handling single WiFi-CSI input. Additionally, we are surprised to find that prioritizing a particular modality does not degrade the model’s ability to extract features from the other two modalities. Consequently, the multimodal fusion results are also improved a lot.

XRF55		Accuracy (%)		
(P_R, P_W, P_{RF})		(0.5,0.5,0.8)	(0.5,0.7,0.7)	(0.5,0.9,0.6)
R	82.2%	82.4%	83.9%	
W	29.1%	37.4%	55.7%	
RF	41.6%	41.9%	42.5%	
R+W	85.1%	86.0%	88.2%	
R+RF	84.5%	84.8%	86.5%	
W+RF	50.3%	52.7%	58.1%	
R+W+RF	86.4%	87.3%	89.8%	

Table 3: Comparisons of X-Fi trained with different modality existence lists. The probabilities are shown in decimal form.

MM-Fi		MPJPE (mm)		PA-MPJPE (mm)	
Method	Transformer	X-Fusion	Transformer	X-Fusion	
I	99.6	93.9	65.0	60.3	
L	212.2	167.1	109.6	103.2	
R	138.0	127.4	74.6	69.8	
W	243.3	225.6	112.9	105.3	
L + R	123.4	109.8	69.9	63.4	
L + W	216.3	159.5	112.7	102.7	
I + L + W	96.6	93.0	61.5	59.7	

Table 4: Comparison between transformer-based fusion and X-Fusion on the HPE task..

Comparison between transformer-only fusion and X-Fusion. To assess whether the X-Fusion module’s feature injection mechanism preserves distinctive features from each modality and enhances multi-modal fusion, we replace X-Fusion in X-Fi with a basic transformer encoder consisting of four stacked blocks. We conduct experiments on these variants, with a subset of results analyzed in Table 4 and the full findings provided in the appendix 5. As shown in Table 4, X-Fusion yields better performance on most of the modality combination input. First, when handling single modality input, transformer-based fusion struggles with challenging modalities, whereas X-Fusion effectively captures the distinctive features of each modality. For example, performance with LiDAR input improves by 21.3%. Next, in contrast to transformer-based fusion methods, X-Fusion leverages each modality’s strengths, yielding better fusion results than single-modality inputs. X-Fusion demonstrates superior performance compared to either the LiDAR or WiFi-CSI modality when used individually. Lastly, in the case of multi-modality inputs, the performance of transformer-based fusion is highly dependent on the presence of dominant modalities. For example, adding the RGB modality improves the performance of the LiDAR and WiFi-CSI multi-modal inputs by 119.7 mm with the transformer backbone, whereas the corresponding improvement with X-Fusion is 66.6 mm.

Comparison between X-Fusion and its variants. To evaluate whether the proposed X-Fusion structure, which iterates multiple loops on the same X-Fusion block, is optimal for preserving and fusing multi-modal features, we design two variants. The first employs a layered architecture with four sequentially stacked X-Fusion blocks, where each layer learns new key-value pairs from the multimodal embedding of the previous layer. The second variant is similar, but uses the same key-value pairs across layers, learned from the embedding generated by the modality feature encoder. We conduct experiments on both variants, with full results provided in the appendix 5. On average, the first variant demonstrates a performance improvement of +1.27 mm for MPJPE and -0.7 mm for PA-MPJPE across all modality combinations. The second variant achieves an improvement of +0.93 mm for MPJPE and +0.03 mm for PA-MPJPE. Therefore, considering the computational efficiency and the minor performance differences, we retain the X-Fusion structure where an X-Fusion block is applied iteratively.

4.4 QUALITATIVE RESULTS

To intuitively illustrate the performance of X-Fi on the human sensing tasks, we visualize the estimated human skeleton generated by the model in the HPE task in Figure. 3 and employ the t-SNE method (Van der Maaten & Hinton, 2008) to visualize the multimodal embedding obtained by the X-fusion block for the HAR task in Figure. 4.

Human Pose Estimation. The visualization results for HPE comprise two actions, ‘picking up things’ and ‘throwing,’ each depicted through a sequence of four images. In different rows, we presented the results for the RGB and depth single-modal inputs, the fused results of the RGB and depth multimodal inputs, and the ground truth. To facilitate a clearer comparison between the fused results and the single-modal inputs results, we incorporated blue and orange dashed lines in the fused result images to represent the results of the RGB and depth single-modality inputs, respectively. Through observation, we found that the RGB modality provides more accurate estimations of leg movements, while the depth modality achieves greater accuracy in estimating hand movements. By combining both modalities into a multi-modal input, X-Fi effectively retains the leg movement accuracy from

the RGB modality and the hand movement accuracy from the depth modality, resulting in fused outcomes that are closest to the ground truth.

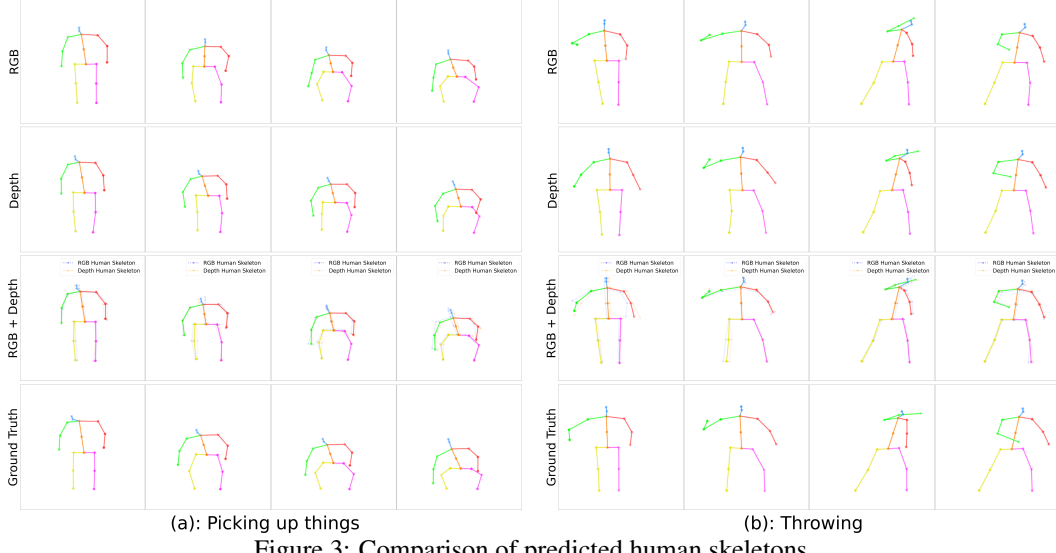


Figure 3: Comparison of predicted human skeletons.

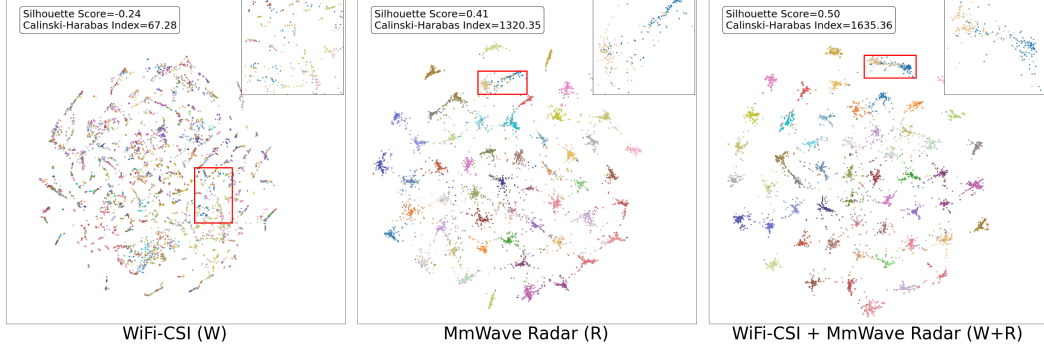


Figure 4: Comparison of multi-modal embedding distribution for HAR. The upper right corner of the image provides an enlarged view of the red-boxed area from the original image.

Human Activity Recognition. The visualization results for HAR includes the multi-modal embedding distributions from WiFi-CSI and mmWave Radar single-modal inputs, as well as the combined WiFi-CSI and mmWave Radar multi-modal inputs. To more closely analyze the distribution of sample points, we zoomed in on a small region containing points from two distinct categories. To quantify the distribution, we used the Silhouette score and Calinski–Harabasz index as indicators of clustering quality. The Silhouette score assesses how well an object fits within its own cluster compared to others, ranging from -1 to 1, with higher values indicating better separation and cohesion. Similarly, higher Calinski–Harabasz index values reflect more distinct clusters. We observed that the multimodal input results exhibit superior feature discriminability. While the mmWave Radar single-modal results demonstrate good classification capability, a closer inspection of the zoomed-in region reveals that the multimodal input results forms tighter clusters. Furthermore, a comparison of the indicator values confirms that the multimodal results outperforms any single-modal results.

5 CONCLUSION

In this paper, we introduce X-Fi, a modality-invariant foundation model designed to overcome the limitations of current human sensing approaches, which often rely on fixed modality combinations. By leveraging a transformer architecture and a novel X-fusion mechanism, X-Fi supports flexible multimodal integration and effectively utilizes distinctive modal information. Our extensive experiments on the MM-Fi and XRF55 datasets demonstrate the model’s superior performance in both

human pose estimation (HPE) and human activity recognition (HAR) tasks. These results highlight X-Fi’s potential to drive advancements in scalable, multimodal human sensing technologies.

REFERENCES

Sizhe An and Umit Y Ogras. Mars: mmwave-based assistive rehabilitation system for smart health-care. *ACM Transactions on Embedded Computing Systems (TECS)*, 20(5s):1–22, 2021.

Sizhe An and Umit Y Ogras. Fast and scalable human pose estimation using mmwave point cloud. In *Proceedings of the 59th ACM/IEEE Design Automation Conference*, pp. 889–894, 2022.

Sizhe An, Yin Li, and Umit Ogras. mri: Multi-modal 3d human pose estimation dataset using mmwave, rgb-d, and inertial sensors. *Advances in Neural Information Processing Systems*, 35: 27414–27426, 2022.

Zhongang Cai, Daxuan Ren, Ailing Zeng, Zhengyu Lin, Tao Yu, Wenjia Wang, Xiangyu Fan, Yang Gao, Yifan Yu, Liang Pan, et al. Humman: Multi-modal 4d human dataset for versatile sensing and modeling. In *European Conference on Computer Vision*, pp. 557–577. Springer, 2022.

Zhongang Cai, Wanqi Yin, Ailing Zeng, Chen Wei, Qingping Sun, Wang Yanjun, Hui En Pang, Haiyi Mei, Mingyuan Zhang, Lei Zhang, et al. Smpler-x: Scaling up expressive human pose and shape estimation. *Advances in Neural Information Processing Systems*, 36, 2024.

Anjun Chen, Xiangyu Wang, Kun Shi, Shaohao Zhu, Bin Fang, Yingfeng Chen, Jiming Chen, Yuchi Huo, and Qi Ye. Immfusion: Robust mmwave-rgb fusion for 3d human body reconstruction in all weather conditions. In *2023 IEEE International Conference on Robotics and Automation (ICRA)*, pp. 2752–2758. IEEE, 2023.

Junchul Chun, Seohee Park, and Myunggeun Ji. 3d human pose estimation from rgb-d images using deep learning method. In *Proceedings of the 2018 International Conference on Sensors, Signal and Image Processing*, pp. 51–55, 2018.

Avigyan Das, Pritam Sil, Pawan Kumar Singh, Vikrant Bhateja, and Ram Sarkar. Mmhar-ensemnet: A multi-modal human activity recognition model. *IEEE Sensors Journal*, 21(10):11569–11576, 2021. doi: 10.1109/JSEN.2020.3034614.

Alexey Dosovitskiy, Lucas Beyer, Alexander Kolesnikov, Dirk Weissenborn, Xiaohua Zhai, Thomas Unterthiner, Mostafa Dehghani, Matthias Minderer, Georg Heigold, Sylvain Gelly, Jakob Uszkoreit, and Neil Houlsby. An image is worth 16x16 words: Transformers for image recognition at scale, 2021. URL <https://arxiv.org/abs/2010.11929>.

Omar Elharrouss, Noor Almaadeed, and Somaya Al-Maadeed. A review of video surveillance systems. *Journal of Visual Communication and Image Representation*, 77:103116, 2021.

Qing Gao, Jinguo Liu, Zhaojie Ju, and Xin Zhang. Dual-hand detection for human–robot interaction by a parallel network based on hand detection and body pose estimation. *IEEE Transactions on Industrial Electronics*, 66(12):9663–9672, 2019.

Shubham Goel, Georgios Pavlakos, Jathushan Rajasegaran, Angjoo Kanazawa, and Jitendra Malik. Humans in 4d: Reconstructing and tracking humans with transformers. In *Proceedings of the IEEE/CVF International Conference on Computer Vision*, pp. 14783–14794, 2023.

Jiaming Han, Kaixiong Gong, Yiyuan Zhang, Jiaqi Wang, Kaipeng Zhang, Dahua Lin, Yu Qiao, Peng Gao, and Xiangyu Yue. Onellm: One framework to align all modalities with language. In *Proceedings of the IEEE/CVF Conference on Computer Vision and Pattern Recognition*, pp. 26584–26595, 2024.

Kaiming He, Xiangyu Zhang, Shaoqing Ren, and Jian Sun. Deep residual learning for image recognition. In *Proceedings of the IEEE conference on computer vision and pattern recognition*, pp. 770–778, 2016.

Catalin Ionescu, Dragos Papava, Vlad Olaru, and Cristian Sminchisescu. Human3. 6m: Large scale datasets and predictive methods for 3d human sensing in natural environments. *IEEE transactions on pattern analysis and machine intelligence*, 36(7):1325–1339, 2013.

Yann LeCun, Léon Bottou, Yoshua Bengio, and Patrick Haffner. Gradient-based learning applied to document recognition. *Proceedings of the IEEE*, 86(11):2278–2324, 1998.

Jialian Li, Jingyi Zhang, Zhiyong Wang, Siqi Shen, Chenglu Wen, Yuexin Ma, Lan Xu, Jingyi Yu, and Cheng Wang. Lidarcap: Long-range marker-less 3d human motion capture with lidar point clouds. In *Proceedings of the IEEE/CVF conference on computer vision and pattern recognition*, pp. 20502–20512, 2022.

Xinyu Li, Bing Shuai, and Joseph Tighe. Directional temporal modeling for action recognition. In *Computer Vision–ECCV 2020: 16th European Conference, Glasgow, UK, August 23–28, 2020, Proceedings, Part VI 16*, pp. 275–291. Springer, 2020.

Jiasen Lu, Dhruv Batra, Devi Parikh, and Stefan Lee. Vilbert: Pretraining task-agnostic visiolinguistic representations for vision-and-language tasks. *Advances in neural information processing systems*, 32, 2019.

Yunze Man, Liang-Yan Gui, and Yu-Xiong Wang. Bev-guided multi-modality fusion for driving perception. In *Proceedings of the IEEE/CVF Conference on Computer Vision and Pattern Recognition*, pp. 21960–21969, 2023.

Timo von Marcard, Gerard Pons-Moll, and Bodo Rosenhahn. Human pose estimation from video and imus. *IEEE Transactions on Pattern Analysis and Machine Intelligence*, 38(8):1533–1547, 2016. doi: 10.1109/TPAMI.2016.2522398.

Marius Memmel, Roman Bachmann, and Amir Zamir. Modality-invariant visual odometry for embodied vision. In *Proceedings of the IEEE/CVF Conference on Computer Vision and Pattern Recognition*, pp. 21549–21559, 2023.

Vinod Nair and Geoffrey E Hinton. Rectified linear units improve restricted boltzmann machines. In *Proceedings of the 27th international conference on machine learning (ICML-10)*, pp. 807–814, 2010.

Jeffrey A Nanzer. A review of microwave wireless techniques for human presence detection and classification. *IEEE Transactions on Microwave Theory and Techniques*, 65(5):1780–1794, 2017.

Duc Thanh Nguyen, Wanqing Li, and Philip O Ogunbona. Human detection from images and videos: A survey. *Pattern Recognition*, 51:148–175, 2016.

Isura Nirmal, Abdelwahed Khamis, Mahbub Hassan, Wen Hu, and Xiaoqing Zhu. Deep learning for radio-based human sensing: Recent advances and future directions. *IEEE Communications Surveys & Tutorials*, 23(2):995–1019, 2021.

Georgios Pavlakos, Luyang Zhu, Xiaowei Zhou, and Kostas Daniilidis. Learning to estimate 3d human pose and shape from a single color image. In *Proceedings of the IEEE conference on computer vision and pattern recognition*, pp. 459–468, 2018.

Charles R Qi, Hao Su, Kaichun Mo, and Leonidas J Guibas. Pointnet: Deep learning on point sets for 3d classification and segmentation. In *Proceedings of the IEEE conference on computer vision and pattern recognition*, pp. 652–660, 2017.

Helei Qiu, Biao Hou, Bo Ren, and Xiaohua Zhang. Spatio-temporal tuples transformer for skeleton-based action recognition. *arXiv preprint arXiv:2201.02849*, 2022.

Yiming Ren, Xiao Han, Chengfeng Zhao, Jingya Wang, Lan Xu, Jingyi Yu, and Yuexin Ma. Livehps: Lidar-based scene-level human pose and shape estimation in free environment. In *Proceedings of the IEEE/CVF Conference on Computer Vision and Pattern Recognition*, pp. 1281–1291, 2024.

Amir Shahroudy, Jun Liu, Tian-Tsong Ng, and Gang Wang. Ntu rgb+ d: A large scale dataset for 3d human activity analysis. In *Proceedings of the IEEE conference on computer vision and pattern recognition*, pp. 1010–1019, 2016.

Ke Sun, Bin Xiao, Dong Liu, and Jingdong Wang. Deep high-resolution representation learning for human pose estimation, 2019. URL <https://arxiv.org/abs/1902.09212>.

Alexander Toshev and Christian Szegedy. Deeppose: Human pose estimation via deep neural networks. In *Proceedings of the IEEE conference on computer vision and pattern recognition*, pp. 1653–1660, 2014.

Laurens Van der Maaten and Geoffrey Hinton. Visualizing data using t-sne. *Journal of machine learning research*, 9(11), 2008.

Ashish Vaswani, Noam Shazeer, Niki Parmar, Jakob Uszkoreit, Llion Jones, Aidan N Gomez, Łukasz Kaiser, and Illia Polosukhin. Attention is all you need. *Advances in neural information processing systems*, 30, 2017.

Michalis Vrigkas, Christophoros Nikou, and Ioannis A Kakadiaris. A review of human activity recognition methods. *Frontiers in Robotics and AI*, 2:28, 2015.

Fei Wang, Yizhe Lv, Mengdie Zhu, Han Ding, and Jinsong Han. Xrf55: A radio frequency dataset for human indoor action analysis. *Proceedings of the ACM on Interactive, Mobile, Wearable and Ubiquitous Technologies*, 8(1):1–34, 2024.

Yuheng Wang, Haipeng Liu, Kening Cui, Anfu Zhou, Wensheng Li, and Huadong Ma. m-activity: Accurate and real-time human activity recognition via millimeter wave radar. In *ICASSP 2021-2021 IEEE International Conference on Acoustics, Speech and Signal Processing (ICASSP)*, pp. 8298–8302. IEEE, 2021.

Zihui Xue and Radu Marculescu. Dynamic multimodal fusion. In *Proceedings of the IEEE/CVF Conference on Computer Vision and Pattern Recognition*, pp. 2575–2584, 2023.

Jianfei Yang, Xinyan Chen, Han Zou, Chris Xiaoxuan Lu, Dazhuo Wang, Sumei Sun, and Lihua Xie. Sensefi: A library and benchmark on deep-learning-empowered wifi human sensing. *Patterns*, 4(3), 2023.

Jianfei Yang, He Huang, Yunjiao Zhou, Xinyan Chen, Yuecong Xu, Shenghai Yuan, Han Zou, Chris Xiaoxuan Lu, and Lihua Xie. Mm-fi: Multi-modal non-intrusive 4d human dataset for versatile wireless sensing. *Advances in Neural Information Processing Systems*, 36, 2024.

Hengshuang Zhao, Li Jiang, Jiaya Jia, Philip HS Torr, and Vladlen Koltun. Point transformer. In *Proceedings of the IEEE/CVF international conference on computer vision*, pp. 16259–16268, 2021.

Jingxiao Zheng, Xinwei Shi, Alexander Gorban, Junhua Mao, Yang Song, Charles R Qi, Ting Liu, Visesh Chari, Andre Cornman, Yin Zhou, et al. Multi-modal 3d human pose estimation with 2d weak supervision in autonomous driving. In *Proceedings of the IEEE/CVF Conference on Computer Vision and Pattern Recognition*, pp. 4478–4487, 2022.

Yunjiao Zhou, He Huang, Shenghai Yuan, Han Zou, Lihua Xie, and Jianfei Yang. Metafi++: Wifi-enabled transformer-based human pose estimation for metaverse avatar simulation. *IEEE Internet of Things Journal*, 10(16):14128–14136, 2023.

A APPENDIX

MM-Fi	MPJPE				PA-MPJPE			
	X-Fi Variants	Transformer Fusion	X-Fusion (iterative)	X-Fusion (stacked)	X-Fusion (stacked, same kv)	Transformer Fusion	X-Fusion (iterative)	X-Fusion (stacked)
I	99.6	93.9	100.6	95.8	65.0	60.3	62.2	61.3
D	109.0	<u>101.8</u>	94.8	<u>104.5</u>	56.1	48.4	50.8	48.8
L	212.2	<u>167.1</u>	184.9	160.2	109.6	103.2	104.7	<u>103.6</u>
R	138.0	127.4	121.2	122.8	74.6	69.8	65.4	<u>66.4</u>
W	243.3	<u>225.6</u>	229.7	224.3	112.9	<u>105.3</u>	105.4	103.2
I + D	89.7	86.1	81.1	84.9	52.9	48.1	50.0	48.1
I + L	96.6	93.0	98.8	<u>93.2</u>	62.4	59.7	60.9	<u>60.2</u>
I + R	93.0	88.8	91.9	<u>89.8</u>	59.1	57.3	<u>57.5</u>	<u>58.3</u>
I + W	96.0	93.0	97.2	<u>94.0</u>	61.9	59.5	60.9	<u>60.5</u>
D + L	<u>97.3</u>	102.5	91.4	97.9	52.3	<u>48.4</u>	49.5	48.0
D + R	<u>94.9</u>	98.0	88.4	96.8	50.6	47.3	48.0	47.3
D + W	<u>95.6</u>	101.8	94.5	98.8	51.4	<u>48.1</u>	49.6	48.0
L + R	<u>123.4</u>	109.8	115.5	106.9	69.9	<u>63.4</u>	64.1	61.7
L + W	216.3	<u>159.5</u>	181.7	156.4	112.7	<u>102.7</u>	103.9	102.5
R + W	126.1	117.2	120.8	<u>117.4</u>	70.0	62.7	63.9	62.7
I + D + L	86.8	84.8	78.6	84.2	52.2	<u>48.2</u>	49.3	48.0
I + D + R	85.2	<u>83.4</u>	78.2	<u>83.8</u>	50.9	47.3	48.7	<u>47.5</u>
I + D + W	85.6	85.3	79.6	<u>84.5</u>	51.5	48.1	49.3	48.1
I + L + R	93.4	88.4	93.0	<u>89.7</u>	59.1	<u>57.2</u>	57.1	58.3
I + L + W	96.6	93.0	98.1	93.0	61.5	59.7	<u>60.1</u>	60.2
I + R + W	93.3	88.5	91.8	<u>90.0</u>	58.8	<u>57.1</u>	57.0	58.4
D + L + R	<u>91.5</u>	96.0	84.8	<u>95.8</u>	50.5	47.3	47.9	47.4
D + L + W	<u>93.0</u>	102.0	88.9	98.1	51.4	<u>48.1</u>	49.2	47.9
D + R + W	<u>90.6</u>	97.0	87.2	97.3	50.4	47.1	47.7	47.3
L + R + W	<u>122.8</u>	107.4	116.0	106.4	70.4	<u>63.1</u>	63.7	61.3
I + D + L + R	84.1	83.5	77.0	83.2	51.2	47.6	48.3	47.6
I + D + L + W	84.7	86.0	78.1	<u>84.2</u>	51.8	<u>48.2</u>	48.9	48.0
I + D + R + W	<u>83.4</u>	84.0	77.9	<u>83.9</u>	50.8	47.6	48.2	47.7
I + L + R + W	93.9	88.6	92.7	<u>89.5</u>	59.1	<u>57.1</u>	56.8	58.4
D + L + R + W	89.4	97.6	84.4	95.8	50.7	47.4	47.7	47.4
I + D + L + R + W	<u>82.9</u>	83.7	76.6	83.1	51.3	47.6	47.9	47.6

Table 5: Full results of the comparison among transformer-based fusion, X-Fusion, and X-Fusion’s variants.

A.1 FEATURE EXTRACTOR PRE-TRAINING.

As mentioned in the main work, to effectively extract informative high-dimensional representations from modal data, we designed modality-specific feature extractors whose backbone structures could be selected based on the data structure of each modality and the characteristics of the datasets. Meanwhile, we employ pre-training techniques to preserve the efficiency of feature extraction. Initially, for each modality, we train an entire model on the respective dataset and task. A portion of the model architecture is then repurposed as the feature extractor, with the corresponding pre-trained weights frozen during subsequent training. For instance, a ResNet-18 model was first trained on RGB images from the MM-Fi dataset to perform HPE. Subsequently, the MLP structure of the model’s output layer was discarded, retaining only the bottleneck blocks serving as the feature extractor. To identify efficient backbone structures, we conducted experiments to validate the performance of various backbone structures on each dataset. The finalized backbones are presented in the following. When utilizing MM-Fi for HPE, we employ the ResNet-18 architecture (He et al., 2016) for both the RGB and Depth modalities, the Point Transformer architecture (Zhao et al., 2021) for LiDAR, the Point Transformer architecture without transition down layers for mmWave point cloud data, and the MetaFi++ architecture (Zhou et al., 2023) for WiFi-CSL. For HAR using MM-Fi, the same backbone architectures are utilized, with the parameters specifically trained for HAR due to the differing feature representation requirements across tasks. When utilizing the XRF55 dataset for HAR, the ResNet-18 architecture is adopted for the RFID, WiFi, and mmWave modalities to maintain consistency with the baseline backbone networks employed in the study (Wang et al., 2024).

Ablation Studies on MM-Fi HAR	Dropout Layer		Positional Encoding	
	Accuracy		Accuracy	
Methods	DPR = 0.3	DPR = 0.0	False	True
I	26.1%	27.4%	25.4%	27.4%
D	46.6%	47.3%	47.0%	47.3%
L	12.8%	32.9%	31.9%	32.9%
R	80.9%	86.0%	85.5%	86.0%
I + D	46.3%	45.2%	45.9%	45.2%
I + L	27.1%	29.8%	30.6%	29.8%
I + R	69.2%	72.4%	74.4%	72.4%
D + L	46.2%	48.4%	49.0%	48.4%
D + R	74.7%	80.2%	78.6%	80.2%
L + R	79.3%	86.7%	87.4%	86.7%
I + D + L	46.1%	46.1%	47.6%	46.1%
I + D + R	67.6%	70.8%	69.9%	70.8%
I + L + R	66.9%	74.4%	75.6%	74.4%
D + L + R	72.6%	80.1%	78.3%	80.1%
I + D + L + R	65.8%	70.0%	70.7%	70.0%

Table 6: Ablation studies on drop out layers and positional encoding layer.

A.2 EVALUATION OF MODALITY-SPECIFIC FEATURES COMBINING METHODS

Our objective is to assess whether concatenation is the most effective method for combining modality-specific features into multi-modal embedding. To investigate this, we conducted a controlled experiment on the MM-Fi HPE task. In this experiment, we compared the concatenation method with the feature addition approach, where the feature values from each modality are summed and then divided by the number of modalities. As demonstrated in the Table 7, the feature addition approach failed to preserve distinctive modality features in the multimodal embeddings, resulting in average performance deteriorations of 15.7 mm on MPJPE and 5.9 mm on PA-MPJPE.

A.3 ABLATION STUDIES

To demonstrate the effectiveness of our proposed modality-invariant foundation model and the corresponding optimization process, we evaluate the impact of dropout layer, positional encoding, and the optimizer choice. And the results are illustrated in Table 6& 7.

To evaluate the effect of dropout layers, we incorporated a dropout layer with a rate of 0.3 into all transformer structures within X-Fi and assessed its performance on the MMFi dataset for the HAR task. The experimental results indicated that the introduction of the dropout layer led to a 4.6% decrease in averaged accuracy. Furthermore, the dropout layer significantly impaired the model’s predictive performance, particularly when handling challenging modalities.

To assess the impact of different optimizer choices on experimental results, we conducted a set of controlled experiments using the SGD optimizer with a learning rate scheduler on the MM-Fi HPE task. The results indicated that the AdamW optimizer facilitated better convergence to a more optimal local minimum, leading to an average performance improvement of xx mm on MPJPE and x mm on PA-MPJPE.

To assess the impact of LiDAR positional encoding, we conducted an experiment by removing the positional encoding structure. The results demonstrated that positional encoding provided a slight improvement in the performance of X-Fi with single-modality input. However, when faced with multi-modal inputs, the model’s performance fluctuated, exhibiting worse results with certain modality combinations while performing better with others.

Ablation Studies on MM-Fi HPE	multi-modal feature combining methods				optimizer choices			
	MPJPE		PA-MPJPE		MPJPE		PA-MPJPE	
Methods	Add	Concate	Add	Concate	SGD	AdamW	SGD	AdamW
I	123.4	93.9	78	60.3	239.1	93.9	165.2	60.3
D	112.5	101.8	54.4	48.4	211.9	101.8	146.3	48.4
L	226.4	167.1	104.2	103.2	243.9	167.1	130.4	103.2
R	144.3	127.4	70.3	69.8	248.2	127.4	148.1	69.8
W	227.7	225.6	104.8	105.3	296.5	225.6	138	105.3
I + D	96.1	86.1	53.4	48.1	166.4	86.1	116.1	48.1
I + L	115.9	93	76.7	59.7	151.2	93	105.1	59.7
I + R	104.3	88.8	63.1	57.3	149.4	88.8	110.9	57.3
I + W	118.7	93	75.8	59.5	144.4	93	102.8	59.5
D + L	108.9	102.5	53.5	48.4	140.1	102.5	95.8	48.4
D + R	106.6	98	52.8	47.3	147.8	98	106.3	47.3
D + W	110.6	101.8	53.5	48.1	136.6	101.8	99.1	48.1
L + R	135.8	109.8	67.5	63.4	166.6	109.8	108.3	63.4
L + W	210.5	159.5	102.9	102.7	184.3	159.5	113.5	102.7
R + W	131.7	117.2	67.4	62.7	192.5	117.2	117.5	62.7
I + D + L	94.4	84.8	53.1	48.2	127	84.8	87.6	48.2
I + D + R	93.4	83.4	52.4	47.3	136.2	83.4	92.9	47.3
I + D + W	96	85.3	53	48.1	124.5	85.3	88	48.1
I + L + R	101.4	88.4	62.5	57.2	121.5	88.4	85.5	57.2
I + L + W	114.5	93	75.4	59.7	121	93	87.1	59.7
I + R + W	102.7	88.5	62.2	57.1	127	88.5	90.2	57.1
D + L + R	105.2	96	52.4	47.3	125.8	96	88.6	47.3
D + L + W	108.5	102	53.2	48.1	128.1	102	91	48.1
D + R + W	105.8	97	52.4	47.1	127.9	97	91.4	47.1
L + R + W	128.1	107.4	66.9	63.1	164.9	107.4	104.5	63.1
I + D + L + R	92.2	83.5	52.2	47.6	107.4	83.5	76.6	47.6
I + D + L + W	94.4	86	53	48.2	106.2	86	77.2	48.2
I + D + R + W	93.5	84	52.2	47.6	115.9	84	79.3	47.6
I + L + R + W	100.3	88.6	62.3	57.1	113.6	88.6	80.5	57.1
D + L + R + W	104.8	97.6	52.2	47.4	125	97.6	88.5	47.4
I + D + L + R + W	92.3	83.7	52.1	47.6	101.2	83.7	73.6	47.6

Table 7: Ablation studies on comparing multi-modal features combininng methods and optimizer choices.